Available online at www.sciencedirect.com
SCIENCE DIRECT®
Journal of Organometallic Chemistry 670 (2003) 56–65
Journal of Organometallic Chemistry
www.elsevier.com/locate/jorganchem

Organometallic complexes for nonlinear optics Part 31. Cubic hyperpolarizabilities of ferrocenyl-linked gold and ruthenium complexes☆

Stephanie K. Hurst [a], Mark G. Humphrey [a,*], Joseph P. Morrall [a], Marie P. Cifuentes [a], Marek Samoc [b], Barry Luther-Davies [b], Graham A. Heath [c], Anthony C. Willis [c]

[a] Department of Chemistry, Australian National University, Canberra, ACT 0200, Australia
[b] Australian Photonics Cooperative Research Centre, Laser Physics Centre, Research School of Physical Sciences and Engineering, Australian National University, Canberra, ACT 0200, Australia
[c] Research School of Chemistry, Australian National University, Canberra, ACT 0200, Australia

Received 18 September 2002; accepted 26 October 2002

Abstract

The complexes [Fe{η-C_5H_4–(*E*)–CH=CH–4-C_6H_4C≡CX}$_2$] [X = $SiMe_3$ (**1**), H (**2**), Au(PCy_3) (**3**), Au(PPh_3) (**4**), Au(PMe_3) (**5**), RuCl(dppm)$_2$ (**7**), RuCl(dppe)$_2$ (**8**)] and [Fe{η-C_5H_4–(*E*)–CH=CH–4-C_6H_4CH=CRuCl(dppm)$_2$}$_2$](PF_6)$_2$ (**6**) have been prepared and the identities of **1** and **7** confirmed by single-crystal X-ray structural studies. Complexes **1**–**8** exhibit reversible oxidation waves in their cyclic voltammograms attributed to the $Fe^{II/III}$ couple of the ferrocenyl groups, **6**–**8** also showing reversible (**7**, **8**) or non-reversible (**6**) processes attributed to Ru-centered oxidation. Cubic nonlinearities at 800 nm by the Z-scan method are low for **1**–**5**; in contrast, complexes **6** and **7** exhibit large negative γ_{real} and large γ_{imag} values. A factor of 4 difference in $|\gamma|$ and two-photon absorption cross-section σ_2 values for **6** and **7** suggest that they have potential as protically switchable NLO materials.

Keywords: Iron; Ruthenium; Gold; Hyperpolarizability; Acetylide; Electrochemistry; Nonlinear optics

1. Introduction

The nonlinear optical (NLO) properties of organometallic complexes have attracted significant attention recently [2,3], with ferrocenyl and alkynylmetal complexes being the most intensively studied. Combining ferrocenyl and alkynylmetal units in a "supermolecule" is of interest, and ferrocenyl-terminated dialkynylmetal complexes have been reported, the bridging ruthenium bisacetylide influencing ground-state electronic communication between the terminal ferrocenyl groups [4,5]. We were intrigued by the possibility of reversing this design composition and employing an appropriately functionalized 1,1′-disubstituted ferrocene group as the bridge between two metal alkynyl units. Reported herein are synthetic procedures to bis(4-ethynylstyryl)-functionalized ferrocene, its complexation to gold and ruthenium centers, and electrochemical, linear and NLO properties of the resultant complexes.

2. Experimental

All reactions were performed under a nitrogen atmosphere with the use of standard Schlenk techniques. Dichloromethane and triethylamine were dried by distilling over calcium hydride, diethyl ether and tetrahydrofuran (THF) were dried by distilling over sodium–benzophenone, and other solvents were used as received. Petrol refers to a fraction of boiling range 60–80 °C. Chromatography was carried out on silica gel (230–400-mesh ASTM) or basic ungraded alumina.

☆ For Part 30, see Ref. [1].

* Corresponding author. Tel.: +61-2-6125-2927; fax: +61-2-6125-0760.
E-mail address: mark.humphrey@anu.edu.au (M.G. Humphrey).

0022-328X/02/$ - see front matter © 2002 Elsevier Science B.V. All rights reserved.
PII: S0022-328X(02)02131-9

The following reagents were prepared by the literature procedures: [AuCl(PPh$_3$)] [6], [AuCl(PMe$_3$)] [7], [AuCl(PCy$_3$)] [8], [Fe(η-C$_5$H$_4$–(*E*)–CH=CH–4-C$_6$H$_4$I)$_2$] [9], *cis*-[RuCl$_2$(dppm)$_2$] and *cis*-[RuCl$_2$(dppe)$_2$] [10]. Me$_3$SiC≡CH (Aldrich), [PdCl$_2$(PPh$_3$)$_2$] (PMO), CuI (Aldrich), NH_4PF_6 (Aldrich) and tetra-*n*-butylammonium fluoride (Aldrich) were used as received.

Secondary ion mass spectra (SIMS) were recorded using a VG ZAB 2SEQ instrument (30 kV Cs^+ ions, current 1 mA, accelerating potential 8 kV, 3-nitrobenzyl alcohol matrix) at the Research School of Chemistry, Australian National University; peaks are reported as *m*/*z* (assignment, relative intensity). Microanalyses were carried out at the Research School of Chemistry, Australian National University. Infrared spectra were recorded either as 1% KBr discs or dichloromethane solutions using a Perkin–Elmer System 2000 FT-IR. ^{1}H- and ^{31}P-NMR spectra were recorded using a Varian Gemini-300 FT-NMR spectrometer and are referenced to residual chloroform (7.24 ppm) or external 85% H_3PO_4 (0.0 ppm), respectively. The assignments follow the numbering scheme shown in Fig. 1. UV–Vis spectra of solutions were recorded in THF in 1 cm quartz cells using a Cary 5 spectrophotometer. Cyclic voltammetry measurements were recorded using a MacLab 400 interface and MacLab potentiostat from ADInstruments. The supporting electrolyte was 0.1 M $(NBu^n_4)PF_6$ in distilled, deoxygenated CH_2Cl_2. Solutions containing ca. 1×10^{-3} M complex were maintained under argon. Measurements were carried out at room temperature using platinum disc working-, platinum wire auxiliary- and Ag–AgCl reference-electrodes, such that the ferrocene–ferrocenium redox couple was located at 0.56 V (peak separation around 0.09 V). Scan rates were typically 100 mV s^{-1}.

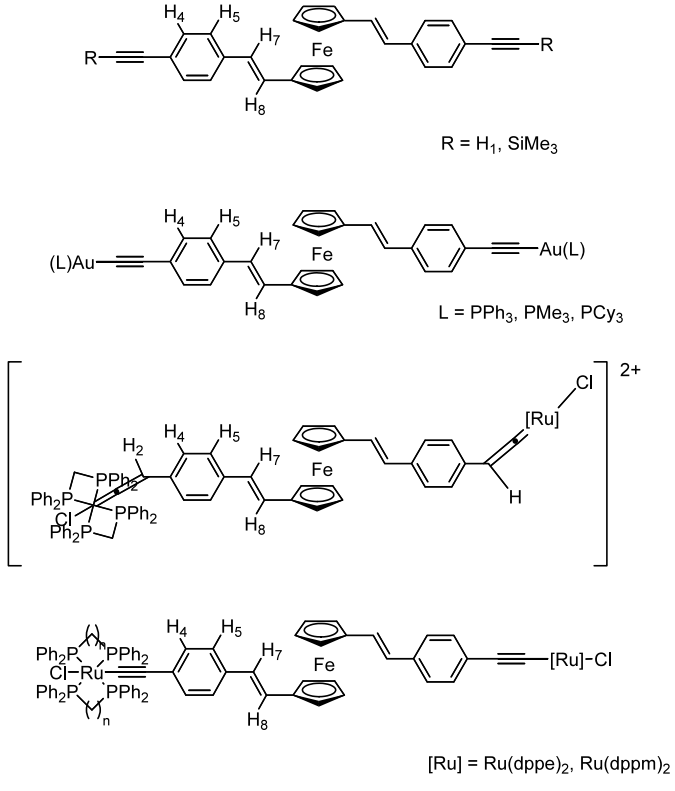

Fig. 1. Numbering scheme for NMR spectral assignments for compounds **1**–**8**.

2.1. Synthesis of [Fe{η-C$_5$H$_4$–(*E*)–CH=CH–4-C$_6$H$_4$C≡CSiMe$_3$}$_2$] (*1*)

[Fe{η-C$_5$H$_4$–(*E*)–CH=CH–4-C$_6$H$_4$I}$_2$] (540 mg, 0.84 mmol), Me$_3$SiC≡CH (0.48 ml, 3.36 mmol), [PdCl$_2$(PPh$_3$)$_2$] (25 mg) and CuI (10 mg) were stirred together in triethylamine (80 ml) for 8 h. The solution was then filtered through a silica plug and the solvent was reduced in volume under vacuum to yield the red product (402 mg, 82%). Anal. Calc. for C$_{36}$H$_{38}$FeSi$_2$: C 74.20, H 6.57%. Found: C 73.62, H 6.16%. IR (CH_2Cl_2) ν(C≡C): 2153 cm^{-1}. UV–Vis: λ (THF) 468 nm, ε 4700 M^{-1} cm^{-1}, 345 nm, ε 52 600 M^{-1} cm^{-1}. ^{1}H-NMR (δ, 300 MHz, $CDCl_3$): 0.25 (s, 18H, Me), 4.26 (m, 4H, C$_5$H$_4$), 4.39 (m, 4H, C$_5$H$_4$), 6.56 (d, J_{HH} = 16 Hz, 2H, H$_7$), 6.78 (d, J_{HH} = 16 Hz, 2H, H$_8$), 7.20 (d, J_{HH} = 8 Hz, 4H, H$_4$), 7.34 (d, J_{HH} = 8 Hz, 4H, H$_5$). SIMS; 582 ([M]$^+$, 100), 567 ([M−Me]$^+$, 5), 319 ([M−(C$_5$H$_4$CH=CHC$_6$H$_4$C≡CSiMe$_3$)]$^+$, 40). A crystal suitable for an X-ray diffraction study was obtained by slow evaporation of a CH_2Cl_2 solution.

2.2. Synthesis of [Fe{η-C$_5$H$_4$–(*E*)–CH=CH–4-C$_6$H$_4$C≡CH}$_2$] (*2*)

[Fe{η-C$_5$H$_4$–(*E*)–CH=CH–4-C$_6$H$_4$C≡CSiMe$_3$}$_2$] (**1**) (400 mg, 0.69 mmol) and NBu^n_4F (1 ml, 1 M solution in THF) were stirred together in dichloromethane (40 ml) for 2 h. The solution was then filtered through an alumina plug and the solvent was reduced in volume under vacuum to yield the red product (256 mg, 85%). IR (CH_2Cl_2) ν(C≡C): 2106 cm^{-1}, ν(≡CH) 3297 cm^{-1}. UV–Vis: λ (THF) 469 nm, ε 2600 M^{-1} cm^{-1}, 341 nm, ε 30 400 M^{-1} cm^{-1}. ^{1}H-NMR (δ, 300 MHz, $CDCl_3$): 3.11 (s, 2H, H$_1$), 4.26 (m, 4H, C$_5$H$_4$), 4.41 (m, 4H, C$_5$H$_4$), 6.54 (d, J_{HH} = 16 Hz, 2H, H$_7$), 6.72 (d, J_{HH} = 16 Hz, 2H, H$_8$), 7.17 (d, J_{HH} = 8 Hz, 4H, H$_4$), 7.32 (d, J_{HH} = 8 Hz, 4H, H$_5$). SIMS: 438 ([M]$^+$, 100), 247 ([M−(C$_5$H$_4$CH=CHC$_6$H$_4$C≡CH)]$^+$, 55). It proved impossible to obtain satisfactory microanalytical data due to slow complex decomposition over a period of days.

2.3. Synthesis of [Fe{η-C$_5$H$_4$–(*E*)–CH=CH–4-C$_6$H$_4$C≡CAu(PCy$_3$)}$_2$] (*3*)

[AuCl(PCy$_3$)] (200 mg, 0.39 mmol), [Fe{η-C$_5$H$_4$–(*E*)–CH=CH–4-C$_6$H$_4$C≡CH}$_2$] (**2**) (92 mg, 0.21 mmol) and CuI (5 mg) were stirred in a solution of

sodium methoxide in methanol (0.1 M, 15 ml) and dichloromethane (15 ml) for 12 h. Dichloromethane (50 ml) was added and the solution filtered through a silica plug. The solvent was reduced in volume under vacuum to yield the red product (184 mg, 63%). Anal. Calc. for $C_{66}H_{86}Au_2FeP_2$: C 56.98, H 6.23%. Found: C 56.47, H 5.84%. IR (CH_2Cl_2) ν(C≡C): 2109 cm^{-1}. UV–Vis: λ (THF) 468 nm, ε 4200 $M^{-1}\,cm^{-1}$, 355 nm, ε 63 600 $M^{-1}\,cm^{-1}$. ^{1}H-NMR (δ, 300 MHz, $CDCl_3$): 1.15–2.10 (m, 66H, Cy), 4.22 (m, 4H, C_5H_4), 4.34 (m, 4H, C_5H_4), 6.59 (d, $J_{HH} = 16$ Hz, 2H, H_7), 6.78 (d, $J_{HH} = 16$ Hz, 2H, H_8), 7.21 (d, $J_{HH} = 8$ Hz, 4H, H_4), 7.42 (d, $J_{HH} = 8$ Hz, 4H, H_5). ^{31}P-NMR (δ, 121 MHz, $CDCl_3$): 56.9. SIMS: 1391 ($[M]^+$, 15), 914 ($[M-Au(PCy_3)]^+$, 100), 477 ($[Au(PCy_3)]^+$, 100).

2.4. Synthesis of [Fe{η-C_5H_4–(*E*)–CH=CH–4-C_6H_4C≡CAu(PPh_3)}$_2$] (**4**)

[AuCl(PPh_3)] (200 mg, 0.40 mmol), [Fe{η-C_5H_4–(*E*)–CH=CH–4-C_6H_4C≡CH}$_2$] (**2**) (87 mg, 0.20 mmol) and CuI (5 mg) were stirred in a solution of sodium methoxide in methanol (0.1 M, 15 ml) and dichloromethane (15 ml) for 12 h. Dichloromethane (50 ml) was added and the solution filtered through a silica plug. The solvent was reduced in volume under vacuum to yield the red product (183 mg, 87%). Anal. Calc. for $C_{66}H_{50}Au_2FeP_2$: C 58.51, H 3.72%. Found: C 58.25, H 3.90%. IR (CH_2Cl_2) ν(C≡C): 2107 cm^{-1}. UV–Vis: λ (THF) 465 nm, ε 5100 $M^{-1}\,cm^{-1}$, 352 nm, ε 72 600 $M^{-1}\,cm^{-1}$. ^{1}H-NMR (δ, 300 MHz, $CDCl_3$): 4.23 (m, 4H, C_5H_4), 4.35 (m, 4H, C_5H_4), 6.60 (d, $J_{HH} = 16$ Hz, 2H, H_7), 6.82 (d, $J_{HH} = 16$ Hz, 2H, H_8), 7.26 (d, $J_{HH} = 9$ Hz, 4H, H_4), 7.30–7.60 (m, 34H, Ph + H_5). ^{31}P-NMR (δ, 121 MHz, $CDCl_3$): 42.8. SIMS: 1355 ($[M]^+$, 5), 721 ($[Au(PPh_3)_2]^+$, 35), 459 ($[AuPPh_3]^+$, 45).

2.5. Synthesis of [Fe{η-C_5H_4–(*E*)–CH=CH–4-C_6H_4C≡CAu(PMe_3)}$_2$]·CH_2Cl_2 (**5**)

[AuCl(PMe_3)] (200 mg, 0.65 mmol), [Fe{η-C_5H_4–(*E*)–CH=CH–4-C_6H_4C≡CH}$_2$] (**2**) (142 mg, 0.32 mmol) and CuI (5 mg) were stirred in a solution of sodium methoxide in methanol (0.1 M, 15 ml) and dichloromethane (15 ml) for 12 h. Dichloromethane (60 ml) was added and the solution filtered through a silica plug. The solvent was reduced in volume under vacuum to yield the red product (172 mg, 54%). Anal. Calc. for $C_{37}H_{40}Au_2Cl_2FeP_2$: C 41.64, H 3.78%. Found: C 40.58, H 4.40%. IR (CH_2Cl_2) ν(C≡C): 2107 cm^{-1}. UV–Vis λ (THF): 463 nm, ε 3200 $M^{-1}\,cm^{-1}$, 350 nm, ε 43 100 $M^{-1}\,cm^{-1}$. ^{1}H-NMR (δ, 300 MHz, $CDCl_3$): 1.51 (d, $J_{HH} = 10$ Hz, 18H, Me), 4.22 (m, 4H, C_5H_4), 4.34 (m, 4H, C_5H_4), 5.27 (s, 2H, CH_2Cl_2), 6.59 (d, $J_{HH} = 16$ Hz, 2H, H_7), 6.79 (d, $J_{HH} = 16$ Hz, 2H, H_8), 7.24 (d, $J_{HH} = 8$ Hz, 4H, H_4), 7.40 (d, $J_{HH} = 8$ Hz, 4H, H_5). ^{31}P-NMR (δ, 121 MHz, $CDCl_3$): 1.7. SIMS: 349 ($[Au(PMe_3)_2]^+$, 10), 273 ($[Au(PMe_3)]^+$, 100).

2.6. Synthesis of [Fe{η-C_5H_4–(*E*)–CH=CH–4-C_6H_4CH=CRuCl(dppm)$_2$}$_2$](PF$_6$)$_2$·CH_2Cl_2 (**6**)

cis-[$RuCl_2$(dppm)$_2$] (255 mg, 0.27 mmol), [Fe{η-C_5H_4–(*E*)–CH=CH–4-C_6H_4C≡CH}$_2$] (**2**) (59 mg, 0.14 mmol) and NH_4PF_6 (88 mg, 0.27 mmol) were stirred in refluxing dichloromethane (35 ml) for 12 h. The material was cooled and petrol (50 ml) was added, and the precipitate was collected on a sintered glass funnel and washed with diethyl ether (100 ml) to give the pale red product (248 mg, 72%). Anal. Calc. for $C_{131}H_{112}Cl_2F_{12}FeP_{10}Ru_2$: C 59.97, H 4.30%. Found: C 59.42, H 4.09%. IR (KBr) ν(PF): 838 cm^{-1}. UV–Vis λ (THF): 383 nm, ε 31 400 $M^{-1}\,cm^{-1}$. ^{1}H-NMR (δ, 300 MHz, $CDCl_3$): 3.10 (m, 2H, H_2), 4.20 (m, 4H, C_5H_4), 4.35 (m, 4H, C_5H_4), 5.12 (m, 4H, PCH_2P), 5.27 (s, 2H, CH_2Cl_2), 5.34 (m, 4H, PCH_2P), 7.35–7.60 (m, 92H, Ph + H_7 + H_8 + C_6H_4). ^{31}P-NMR (δ, 121 MHz, $CDCl_3$): −14.4. SIMS: 2393 ($[M-PF_6]^+$, 40), 2247 ($[M-2H-2PF_6]^+$, 20), 1342 ($[M-RuCl(dppm)_2]^+$, 80), 869 ($[Ru(dppm)_2-H]^+$, 100).

2.7. Synthesis of [Fe{η-C_5H_4–(*E*)–CH=CH–4-C_6H_4C≡CRuCl(dppm)$_2$}$_2$]·CH_2Cl_2 (**7**)

[Fe{η-C_5H_4–(*E*)–CH=CH–4-C_6H_4CH=CRuCl(dppm)$_2$}$_2$](PF$_6$)$_2$·CH_2Cl_2 (**6**) (205 mg, 80.0 μmol) and triethylamine (1 ml) were stirred in dichloromethane (25 ml) for 2 h. The solution was filtered through an alumina plug with dichloromethane. The solvent was reduced in volume under reduced pressure to yield the red product (169 mg, 93%). Anal. Calc. for $C_{131}H_{110}Cl_2FeP_8Ru_2$: C 67.47, H 4.75%. Found: C 67.92, H 5.19%. IR (CH_2Cl_2) ν(C≡C): 2073 cm^{-1}. UV–Vis λ (THF): 397 nm, ε 74 500 $M^{-1}\,cm^{-1}$. ^{1}H-NMR (δ, 300 MHz, $CDCl_3$): 4.21 (m, 4H, C_5H_4), 4.32 (m, 4H, C_5H_4), 4.88 (m, 8H, PCH_2P), 5.27 (s, 2H, CH_2Cl_2), 6.06 (d, $J_{HH} = 8$ Hz, 4H, H_4), 6.57 (d, $J_{HH} = 16$ Hz, 2H, H_7), 6.67 (d, $J_{HH} = 16$ Hz, 2H, H_8), 6.99 (d, $J_{HH} = 8$ Hz, 4H, H_5), 7.03–7.60 (m, 80H, Ph). ^{31}P-NMR (δ, 121 MHz, $CDCl_3$): −5.9. SIMS: 2248 ($[M+H]^+$, 40), 905 ($[RuCl(dppm)_2]^+$, 50), 869 ($[Ru(dppm)_2$-$H]^+$, 100). A crystal suitable for an X-ray diffraction study was obtained by slow diffusion of *n*-heptane into a CH_2Cl_2 solution of **7**.

2.8. Synthesis of [Fe{η-C_5H_4–(*E*)–CH=CH–4-C_6H_4C≡CRuCl(dppe)$_2$}$_2$] (**8**)

cis-[$RuCl_2$(dppe)$_2$] (300 mg, 0.31 mmol), [Fe{η-C_5H_4–(*E*)–CH=CH–4-C_6H_4C≡CH}$_2$] (**2**) (68 mg, 0.15 mmol) and NH_4PF_6 (101 mg, 0.31 mmol) were stirred in refluxing dichloromethane (40 ml) for 6 h. The solution

was cooled and triethylamine (1 ml) was added and stirring continued for 10 min. Petrol (50 ml) was added and the precipitated material was adsorbed onto an alumina column. Diethyl ether (300 ml) was used to remove *trans*-[$RuCl_2(dppe)_2$], and the red product was eluted with dichloromethane (200 ml) (275 mg, 77%). Anal. Calc. for $C_{134}H_{114}Cl_2FeP_8Ru_2$: C 69.88, H 5.08%. Found: C 69.32, H 5.29%. IR (CH_2Cl_2) ν(C≡C): 2065 cm^{-1}. UV–Vis: λ (THF) 388 nm, ε 52 300 M^{-1} cm^{-1}. ^{1}H-NMR (δ, 300 MHz, $CDCl_3$): 2.65 (m, 16H, PCH_2), 4.28 (m, 4H, C_5H_4), 4.40 (m, 4H, C_5H_4), 6.60–6.80 (m, 8H, $H_4+H_7+H_8$), 6.90–7.60 (m, 84H, $Ph+H_5$). ^{31}P-NMR (δ, 121 MHz, $CDCl_3$): 50.1. SIMS: 2267 ($[M-Cl]^+$, 5), 1368 ($[M-RuCl(dppe)_2]^+$, 5), 896 ($[Ru(dppe)_2-2H]^+$, 100).

2.9. X-ray structure determinations of compounds 1 and 7

The crystal and refinement data for compounds **1** and **7** are summarized in Table 1. For each study, a single crystal was mounted on a fine glass capillary, and data were collected at 200 K on a Nonius KappaCCD diffractometer using graphite-monochromated Mo–K_α ($\lambda = 0.71073$ Å). The unit cell parameters were obtained by least-squares refinement [11] of N_{cell} reflections with $2^\circ \leq \theta \leq 25^\circ$. The reduced data [11] were corrected for absorption using numerical methods [12] implemented from within MAXUS [13]; equivalent reflections were merged. Structure **1** was solved by heavy-atom Patterson methods [14] and redefined using the software package TEXSAN [15]. Structure **7** was redefined using CRYSTALS [16].

For **1**, all non-hydrogen atoms were refined with anisotropic displacement factors. Hydrogen atoms were included in the refinement at idealized positions, which were frequently recalculated. The absolute structure was established by refinement of the Flack enantiomorph-polarity parameter. The final value suggests that the crystal may be partially twinned. Note that, for this space group, the unit cell contains a racemic mix of molecules.

As the structure of **7** was solved, various species were revealed. First, the $C_{130}H_{108}Cl_2FeP_8Ru_2$ molecule was identified. The Fe atom lies on a crystallographic twofold axis and the two halves of the molecule are related by this symmetry operation. Next, 10 atom sites forming a zigzag chain were located across an inversion centre. This would appear to be a disordered *n*-heptane molecule of solvation, with the C atoms occupying any seven adjacent sites. If these were selected totally randomly, C(501) should have an occupancy of 1.0, C(502) at 1.0, C(503) at 0.75, C(504) at 0.50 and C(505) at 0.25. If restricted to commence from an end, the respective numbers would be 1.0, 1.0, 0.5, 0.5, and 0.5. A refinement cycle was run letting the individual occupancies vary, but with a common isotropic displacement factor. The final values were 0.98, 0.90, 0.67, 0.61, and 0.45, suggesting a combination of packing alternatives. Consequently, in the final model, the occupancy of C(501) was set at 1.0, C(502) at 1.0, C(504) at 0.5 and the occupancies of C(503) and C(505) were refined to sum to 1.0, and individual isotropic displacement parameters were used. Another chain of atoms was also located, this time seven sites about a twofold axis. This appears to be a *n*-heptane molecule of solvation, but not of full occupancy, and consequently these atoms have been refined with a common occupancy parameter (final value 0.75(4)). Individual isotropic displacement parameters were used for these atoms too. Finally, an isolated atom was discovered which has been interpreted to be a water molecule of solvation. The displacement parameters for this atom are quite large. This might suggest that the occupancy should be less than unity, but alternatively could indicate that the molecule is genuinely not well placed within this space in the structure, and so this matter was not pursued. Hydrogen atoms of the $C_{130}H_{108}Cl_2FeP_8Ru_2$ molecule were included at idealized positions and ride on the atoms to which they were bonded. Other hydrogen atoms were not included. Distances and angles within the solvate molecules are not reliable.

Table 1
Crystal data and structure refinement details for **1** and **7**

	1	**7**
Empirical formula	$C_{36}H_{38}FeSi_2$	$C_{130}H_{108}Cl_2FeP_8Ru_2 \cdot 1.75(C_7H_{16}) \cdot 2(H_2O)$
Molecular weight	582.71	2458.35
Crystal system	Orthorhombic	Monoclinic
Space group	$Pca2_1$	$C2/c$
a (Å)	11.4549(2)	42.5913(11)
b (Å)	5.8778(1)	11.3049(3)
c (Å)	46.9739(9)	26.1606(7)
β (°)		95.009(1)
V (Å^3)	3162.7(2)	12548.0(6)
D_{calc} (g cm^{-3})	1.224	1.301
Crystal size (mm^3)	0.42 × 0.33 × 0.03	0.45 × 0.30 × 0.15
μ (mm^{-1})	0.575	0.548
N_{cell}	38 919	314 151
$N_{collected}$	16 876	50 160
N_{unique}	4945	11 118
N_{obs}	4321	6306
T_{min}, T_{max}	0.854, 0.983	0.829, 0.954
No. of variables	351	690
R [a]	0.0464 ($I > 3\sigma(I)$)	0.0444 ($I > 3\sigma(I)$)
R_w [b]	0.0646 ($I > 3\sigma(I)$)	0.0519 ($I > 3\sigma(I)$)
Weighting scheme, w	$[\sigma^2(F_o)+0.00063\lvert F_o\rvert^2]^{-1}$	[c]
$(\Delta\rho)_{min}$ (e Å^{-3})	−0.50	−0.38
$(\Delta\rho)_{max}$ (e Å^{-3})	0.56	0.87

[a] $R = \Sigma\lvert\lvert F_o\rvert - \lvert F_c\rvert\rvert / \Sigma\lvert F_o\rvert$.
[b] $R_w = [(\Sigma w(\lvert F_o\rvert - \lvert F_c\rvert^2)/\Sigma w F_o^2)]^2$.
[c] Chebyshev polynomial with three parameters [30].

The final cycles of full-matrix least-squares refinement were based on N_{obs} reflections and converged to R and R_w.

2.10. Optical spectroscopy studies

Electronic spectra (45.4×10^3 cm^{-1}) were recorded on a Varian Cary 5E UV–Vis-NIR spectrophotometer. Solution spectra of the oxidized species [mM concentration, in CH_2Cl_2 with 0.3 M (NBu^n_4)(PF_6) supporting electrolyte] were obtained at 248 K by electrogeneration (Thompson 424 potentiostat) at a Pt gauze working electrode within an optically transparent thin-layer electrochemical (OTTLE) cell (Pt auxiliary, Ag–AgCl reference electrodes), path length 0.5 mm, mounted within the spectrophotometer. The electrogeneration potential was 0.8 V, 250–300 mV beyond $E_{1/2}$ for each couple, to ensure complete electrolysis. The efficiency and reversibility of each step were tested by applying a sufficiently negative potential to reduce the product.

2.11. Z-scan measurements

Measurements were performed at 800 nm using 100 fs pulses from a system consisting of a Coherent Mira Ti–sapphire laser pumped with a Coherent Verdi cw pump and a Ti–sapphire regenerative amplifier pumped with a frequency-doubled Q-switched pulsed Nd:YAG laser (Spectra Physics GCR) at 30 Hz and employing chirped pulse amplification. THF solutions were examined in a glass cell with a 0.1 cm path length. The Z-scans were recorded at two concentrations for each compound, and the real and imaginary parts of the nonlinear phase change were determined by numerical fitting [17]. The real and imaginary parts of the hyperpolarizability of the solute were then calculated by assuming linear concentration dependencies of the solution susceptibility. The nonlinearities and light intensities were calibrated using measurements of a 1 mm thick silica plate for which the nonlinear refractive index $n_2 = 3 \times 10^{-16}$ cm^2 W^{-1} was assumed.

3. Results and discussion

3.1. Synthesis and characterization of ferrocenyl-linked acetylenes

Thomas et al. [9] have previously reported the synthesis of [Fe{η-C_5H_4–(*E*)–CH=CH–4-C_6H_4I}$_2$]. We have now shown that the iodo substituents can be functionalized; thus, Sonogashira coupling with trimethylsilylacetylene affords the protected alkyne **1**, which can be deprotected with base to give the terminal acetylene **2** (Scheme 1). The new acetylenes were characterized by SI mass spectrometry, UV–Vis, IR and ^{1}H-NMR spectroscopies, and the identity of **1** was confirmed by a single-crystal X-ray diffraction study.

An ORTEP diagram of **1** is displayed in Fig. 2 and selected bond lengths and angles listed in Table 2. Metrical parameters are unexceptional, the Fe–C(1), C(1)–C(6), and C(6)–C(7) bond distances being within the range of previously observed values for (*E*)-ene functionalized ferrocenyl complexes [9,18–20], and consistent with the representation in Scheme 1; the C(1)–C(6)–C(7)–C(8) unit is approximately planar, with deviations likely to be the result of crystal packing forces. The structural study confirms the *E*-configured double bonds and reveals the eclipsed disposition of the cyclopentadienyl ligands. The molecules pack in a "herringbone" fashion in the crystal lattice (Fig. 3).

A number of heterocyclic or aryl-ethenylferrocene complexes have been structurally characterized [21–24], considerably fewer 1,1′-bis(aryl/heterocyclic-ethenyl)ferrocene examples having been reported [24,25]. Preference for *syn* or *anti* disposition of the arylethenyl groups with respect to the ferrocenyl core is influenced by crystal packing forces, and attempts have been made to apply crystal engineering ideas to co-crystallize 1,1′-bis(ethenyl-4-pyridyl)ferrocene and binaphthol in different solvents [25]. In case of **1**, the observed *anti* arrangement possibly arises because unfavorable steric

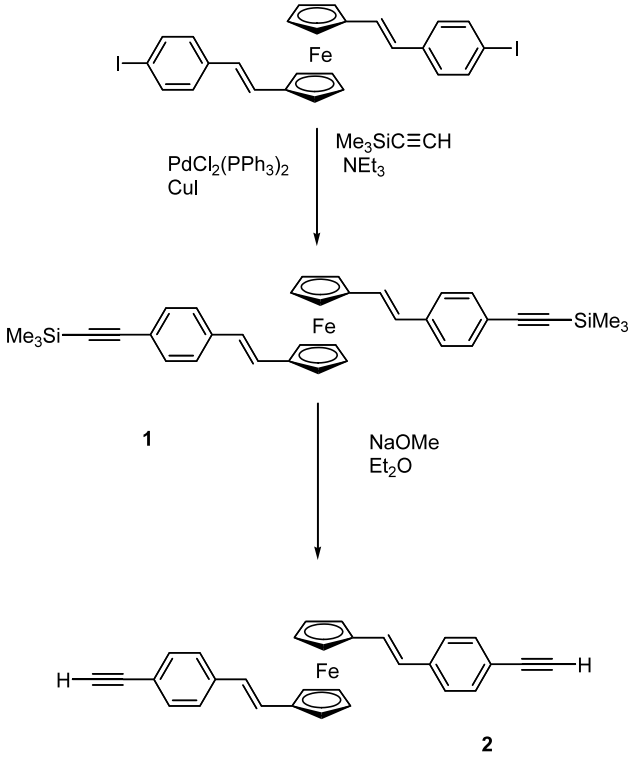

Scheme 1. Synthesis of complexes **1** and **2**.

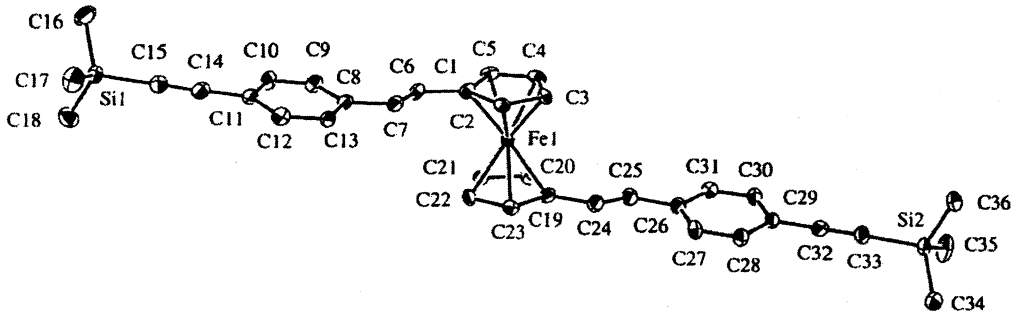

Fig. 2. Molecular geometry and atomic labeling scheme for [Fe{η-C_5H_4–(*E*)–CH=CH–4-C_6H_4C≡CSiMe_3}$_2$] (**1**).

Table 2
Important geometric parameters (Å, °) for complexes **1** and **7**

	1	**7**
Bond distances		
Fe(1)–C(1)	2.069(5)	2.050(5)
C(1)–C(6)	1.467(7)	1.480(7)
C(6)–C(7)	1.342(7)	1.312(8)
C(7)–C(8)	1.459(7)	1.473(7)
C(8)–C(9)	1.385(7)	1.347(8)
C(9)–C(10)	1.356(7)	1.385(8)
C(10)–C(11)	1.407(7)	1.367(8)
C(11)–C(14)	1.435(7)	1.443(7)
C(14)–C(15)	1.190(7)	1.191(6)
Ru(1)–Cl(1)	–	2.4844(11)
Ru(1)–C(15)	–	1.995(4)
Ru(1)–P(1)	–	2.3611(11)
Ru(1)–P(2)	–	2.3369(12)
Ru(1)–P(3)	–	2.3458(12)
Ru(1)–P(4)	–	2.3525(12)
Bond angles		
C(1)–C(6)–C(7)	125.2(4)	125.8(6)
C(6)–C(7)–C(8)	126.2(4)	126.5(6)
C(7)–C(8)–C(9)	123.2(4)	123.1(6)
C(8)–C(9)–C(10)	121.4(4)	121.4(6)
C(9)–C(10)–C(11)	122.2(4)	122.8(6)
C(10)–C(11)–C(14)	118.4(4)	121.5(5)
C(11)–C(14)–C(15)	177.2(5)	176.3(5)
C(14)–C(15)–Si(1)	169.3(5)	–
Cl(1)–Ru(1)–C(15)	–	175.69(14)
Ru(1)–C(15)–C(14)	–	178.6(4)
Cl(1)–Ru(1)–P(1)	–	97.84(4)
Cl(1)–Ru(1)–P(3)	–	86.53(4)
Cl(1)–Ru(1)–P(2)	–	94.94(4)
Cl(1)–Ru(1)–P(4)	–	86.58(4)

effects between trimethylsilyl groups would be experienced in the *syn* disposition.

3.2. Synthesis and characterization of vinylidene and acetylide complexes

The synthetic methodologies employed for the preparation of the new complexes are adaptations of those successfully utilized for the preparation of the corresponding phenylacetylide complexes. Gold phosphine complexes **3**–**5** were prepared in good yield by extending the method of Bruce et al. [7] (Scheme 2); a mixture of the ferrocenyldiyne **2** and the appropriate (phosphine)gold chloride in the presence of base afforded the corresponding acetylide complexes. The (tricyclohexylphosphine)gold complex is significantly more soluble in common organic solvents than its (triphenylphosphine)gold analogue, an important factor when evaluating nonlinearities. The bis{bis(diphenylphosphino)alkane}ruthenium complexes **6**–**8** were prepared by extending the method of Touchard et al. [26] (Scheme 3), a procedure which also permits isolation of the stable vinylidene intermediate. A mixture of either *cis*-[$RuCl_2$(dppm)$_2$] or *cis*-[$RuCl_2$(dppe)$_2$] and excess of the terminal acetylene in the presence of ammonium hexafluorophosphate gives the vinylidene complex, which was isolated in the case of the dppm complex. With the dppe-containing vinylidene complex, excess of acetylene was removed before deprotonation to avoid formation of the bis-alkynyl complex. The vinylidene complexes were deprotonated via addition of base to afford the corresponding acetylides.

The new complexes were characterized by SI mass spectrometry, UV–Vis, IR, ^{1}H- and ^{31}P-NMR spectroscopies. Mass spectra for complexes **1**–**4**, **6** and **7** contain molecular ion or cation signals. The mass spectrum of **8** contains a signal attributable to [M–Cl]$^+$ at highest *m*/*z* value, while that of **5** contains diphosphinegold and phosphinegold cations only. UV–Vis spectra of **1**–**5** contain weak bands in the range 463–469 nm attributed to d–d transitions of the ferrocenyl unit; this band is obscured by the intense ruthenium-centered transition in **6**–**8**. The IR spectra show characteristic *ν*(C≡C) bands (**1**–**5**, **7**, **8**) or a *ν*(PF) band (**6**). ^{31}P-NMR spectra of complexes **6**–**8** contain one singlet resonance, consistent with *trans* geometry at the ruthenium center. The identity of **7** was confirmed by a single-crystal X-ray structural study. An ORTEP diagram is displayed in Fig. 4 and selected bond lengths and angles are listed in Table 2.

Geometric parameters within the 1,1′-di(phenylethenyl)ferrocene unit are comparable to those of **1**. The alkynyl(chloro)bis{bis(diphenylphosphino)methane}ru-

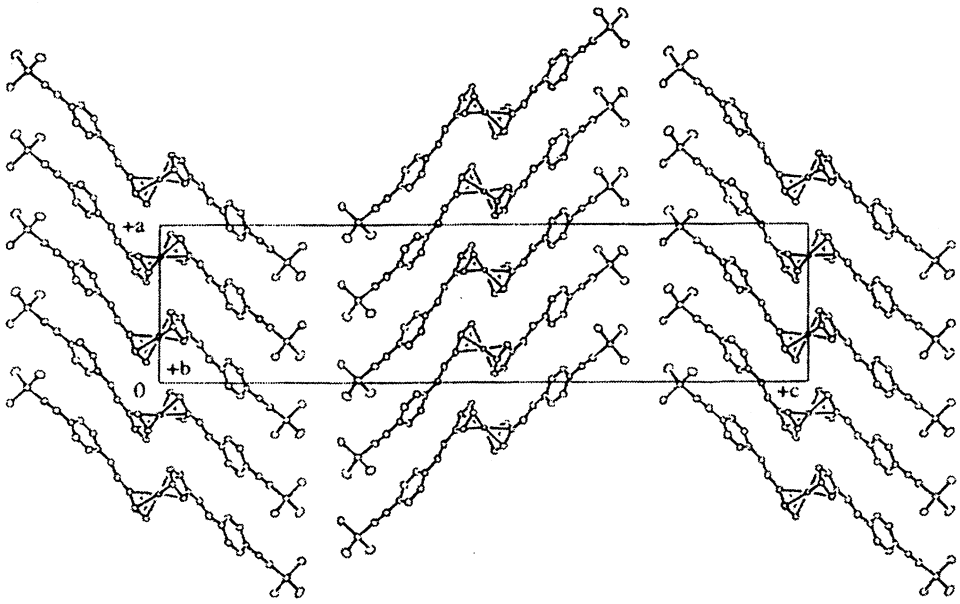

Fig. 3. Cell-packing diagram for [Fe{η-C_5H_4–(*E*)–CH=CH–4-C_6H_4C≡CSiMe_3}$_2$] (**1**).

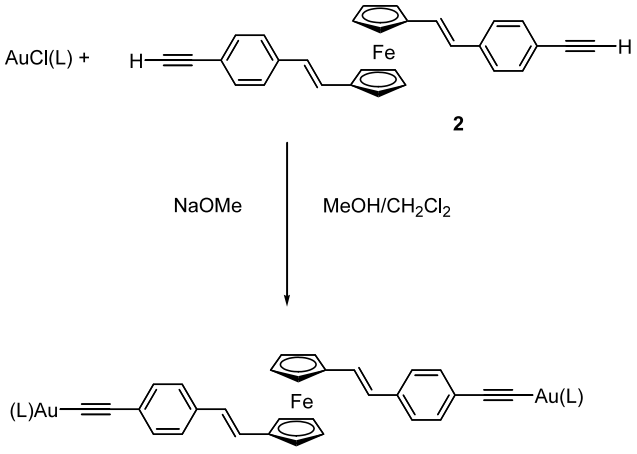

L	Complex
PCy_3	**3**
PPh_3	**4**
PMe_3	**5**

Scheme 2. Syntheses of complexes **3**–**5**.

thenium groups have similar values for metrical parameters to those reported previously in complexes containing this group [27,28]. As with **1**, the arylethenyl units in **7** are observed in an *anti* arrangement with respect to the ferrocenyl core, and the cyclopentadienyl rings are eclipsed.

3.3. Electrochemical studies

Cyclic voltammetry data for complexes **1**–**8** and the precursor [Fe{η-C_5H_4–(*E*)–CH=CH–4-C_6H_4I}$_2$] are gathered in Table 3. The precursor complex has been examined previously [9]; these data are also included in Table 3, and are experimentally similar to data collected under our own laboratory conditions.

Complexes **1**–**5** exhibit a single reversible oxidation wave corresponding to the ferrocenyl unit in the bridging linker. The potential for this ferrocene–ferrocenium couple is similar to that observed for free ferrocene–ferrocenium, the most significant shift in potential being observed for the alkynyl complexes **7** and **8**. Cyclic voltammograms for the ruthenium-containing complexes **6**–**8** also show reversible (**7**, **8**) or non-reversible (**6**) processes attributable to Ru-centered oxidation, at potentials similar to those of monoruthenium alkynyl or vinylidene complexes, respectively [29]. Complexes **1** and **6** were examined in an OTTLE cell, the oxidation resulting in a slight increase in intensity of the low-energy bands in these complexes. Isosbestic points were observed in the spectral progressions (albeit marginal changes) for both transformations (**1**–**6**).

3.4. Cubic hyperpolarizabilities

Third-order nonlinearities for **1**–**7** and the precursor [Fe(η-C_5H_4–(*E*)–CH=CH–4-C_6H_4I)$_2$] were determined by Z-scan at 800 nm, data being collected in Table 4 (complex **8** was insufficiently soluble to afford useful data). The real components of the nonlinearities (γ_{real}) for most of the complexes are negative, and the imaginary components (γ_{imag}) for most are significant, consistent with the two-photon effects contributing to the observed molecular nonlinearities $|\gamma|$; comment on the effect of structural variation on the magnitude of $|\gamma|$ is therefore cautious, particularly in the light of the significant error margins.

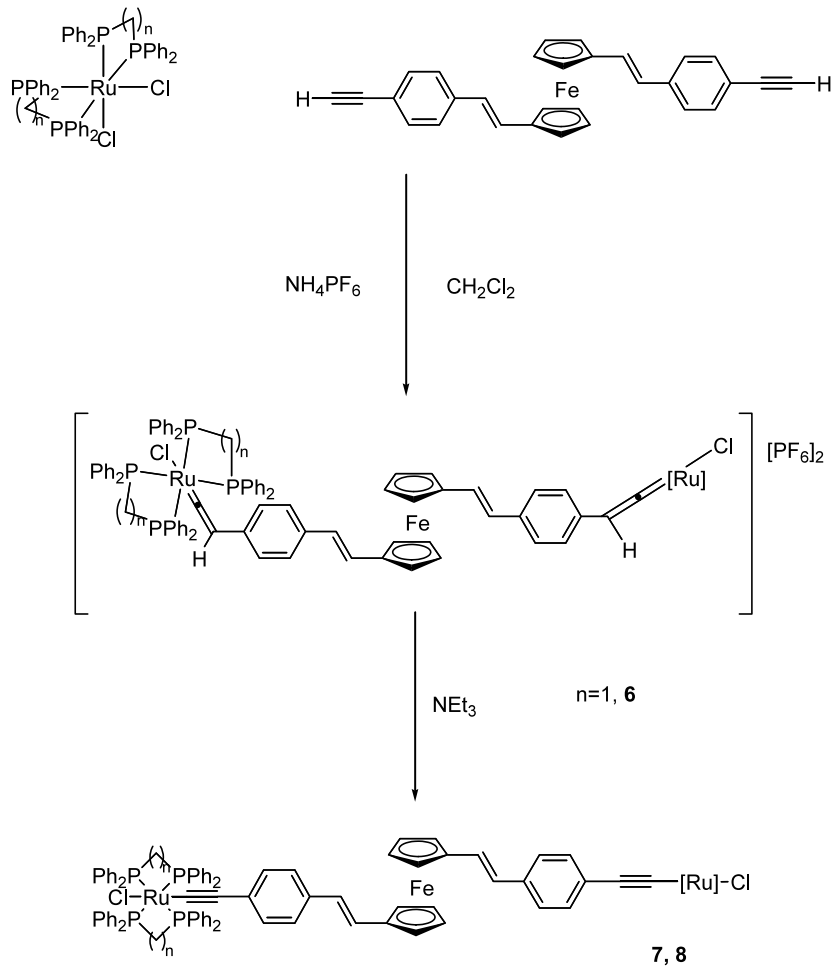

n	Complex
1	**6**
1	**7**
2	**8**

Scheme 3. Syntheses of complexes **6**–**8**.

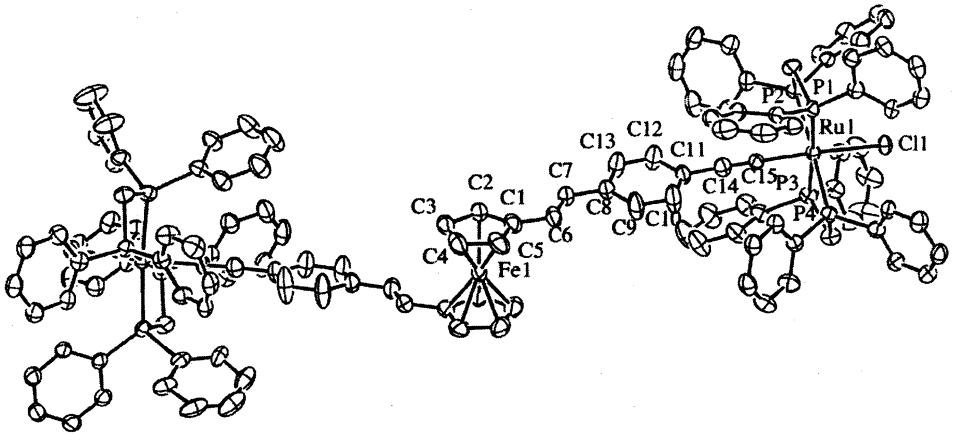

Fig. 4. Molecular geometry and atomic labeling scheme for [Fe{η-C_5H_4–(*E*)–CH=CH–4-C_6H_4C≡CRuCl(dppm)$_2$}$_2$] (**7**).

Table 3
Cyclic voltammetric data for **1–8**

Complex	$E_{1/2}$ ($Fe^{II/III}$) (V)	[i_{pc}/i_{pa}]	$E_{1/2}$ ($Ru^{II/III}$) (V)	[i_{pc}/i_{pa}]	Reference
[Fe(η-C_5H_4–(*E*)–CH=CH–4-$C_6H_4I)_2$]	0.54	1.0	–	–	This work
	0.56	[a]	–	–	[9]
[Fe{η-C_5H_4–(*E*)–CH=CH–4-C_6H_4C≡$CsiMe_3\}_2$] (**1**)	0.55	1.0	–	–	This work
[Fe{η-C_5H_4–(*E*)–CH=CH–4-C_6H_4C≡$CH\}_2$] (**2**)	0.55	1.0	–	–	This work
[Fe{η-C_5H_4–(*E*)–CH=CH–4-C_6H_4C≡$CAu(Pcy_3)\}_2$] (**3**)	0.54	1.0	–	–	This work
[Fe{η-C_5H_4–(*E*)–CH=CH–4-C_6H_4C≡$CAu(PPh_3)\}_2$] (**4**)	0.54	1.0	–	–	This work
[Fe{η-C_5H_4–(*E*)–CH=CH–4-C_6H_4C≡$CAu(Pme_3)\}_2$] (**5**)	0.52	1.0	–	–	This work
[Fe{η-C_5H_4–(*E*)–CH=CH–4-C_6H_4CH=$CRuCl(dppm)_2\}_2$](PF6)2 (**6**) [b]	0.52	1.0	1.25	[c]	This work
[Fe{η-C_5H_4–(*E*)–CH=CH–4-C_6H_4C≡$CRuCl(dppm)_2\}_2$] (**7**)	0.61	1.0	0.44	1.0	This work
[Fe{η-C_5H_4–(*E*)–CH=CH–4-C_6H_4C≡$CRuCl(dppe)_2\}_2$] (**8**)	0.63	1.0	0.49	1.0	This work

Ferrocene–ferrocenium couple (0.56 V) as an internal standard except where specified.
[a] Not specified.
[b] $[Ru(NCMe)_2(acac)_2]$–$[Ru(NCMe)_2(acac)_2]^+$ couple (0.25 V) as an internal standard.
[c] Not reversible.

Nonlinearities for the ferrocenyl complexes **1** and **2** are low. Introduction of terminal (phosphine)gold units in proceeding from **1** to **3** and **5** results in little change in the linear optical absorption spectra and does not result in a significant increase in nonlinearity. The nonlinearity of the triphenylphosphine-containing complex **4** is larger than those of **3** and **5**, suggesting that the additional π-delocalization possibilities of the phenyl substituents on the former are more important for NLO response than the additional electron-donating strength of the alkyl substituents on the latter. Introduction of the ligated ruthenium(II) center (in proceeding to **6** and **7**) results in intense transitions in the UV–Vis spectra close to the second-harmonic wavelength of our Ti–sapphire laser (400 nm) and, as a consequence, complexes **6** and **7** possess large negative γ_{real} and large γ_{imag} values. The prospect of developing "switchable" NLO materials has attracted significant attention recently (see reference [1] and the references cited therein), potential routes to switching including photoisomerization, oxidation–reduction, and protonation–deprotonation. The fourfold difference in $|\gamma|$ and σ_2 values for **6** and **7**, and the facile transformation between ruthenium alkynyl and vinylidene complexes, suggest that they have potential as protically switchable NLO materials.

4. Supplementary material

Crystallographic data for the structural analyses have been deposited with the Cambridge Crystallographic Data Centre, CCDC Nos. 191729 (**1**) and 191730 (**7**).

Table 4
Experimental linear optical spectroscopic and cubic NLO response parameters for **1–8**

Compound	λ_{max} (nm) [ε ($\times 10^4$ M^{-1} cm^{-1})]	γ_{real} (10^{-36} esu)	γ_{imag} (10^{-36} esu)	$\lvert\gamma\rvert$ (10^{-36} esu)	σ_2 (10^{-50} cm^4 s)
[Fe(η-C_5H_4–(*E*)–4CH=$CHC_6H_4I)_2$]	468 [0.6], 336 [8.1]	200±50	100±20	220±50	25
[Fe{η-C_5H_4–(*E*)–4CH=CHC_6H_4C≡ $CsiMe_3\}_2$] (**1**)	468 [0.5], 345 [5.3]	0±50	200±40	200±40	50
[Fe{η-C_5H_4–(*E*)–4CH=CHC_6H_4C≡$CH\}_2$] (**2**)	469 [0.3], 341 [3.0]	−400±250	200±40	450±240	50
[Fe{η-C_5H_4–(*E*)–4CH=CHC_6H_4C≡ $CAu(PCy_3)\}_2$] (**3**)	468 [0.4], 355 [6.4]	−400±500	500±100	640±390	120
[Fe{η-C_5H_4–(*E*)–4CH=CHC_6H_4C≡ $CAu(PPh_3)\}_2$] (**4**)	465 [0.5], 352 [7.3]	−1100±300	300±60	1140±310	70
[Fe{η-C_5H_4–(*E*)–4CH=CHC_6H_4C≡ $CAu(Pme_3)\}_2$] (**5**)	463 [0.3], 350 [4.3]	200±150	0±30	200±150	0
[Fe{η-C_5H_4–(*E*)–4CH=CHC_6H_4CH= $CRuCl(dppm)_2\}_2$]$(PF_6)_2$ (**6**)	383 [3.1]	−3000±1200	2300±800	3800±1400	550
[Fe{η-C_5H_4–(*E*)–4CH=CHC_6H_4C≡ $CRuCl(dppm)_2\}_2$] (**7**)	396 [7.4]	−7100±3000	10600±2000	13000±3000	2500
[Fe{η-C_5H_4–(*E*)–4CH=CHC_6H_4C≡ $CRuCl(dppe)_2\}_2$] (**8**)	388 [5.2]	[a]	[a]	[a]	[a]

All measurements as THF solutions (all complexes are optically transparent at 800 nm). All results are referenced to silica, nonlinear refractive index $n_2 = 3 \times 10^{-16}$ cm^2 W^{-1}.
[a] Insufficiently soluble.

Copies of this information may be obtained, free of charge, from the Director, CCDC, 12 Union Road, Cambridge CB2 1E2, UK (fax: +44-1223-336033; email: deposit@ccdc.cam.ac.uk or www: http://www.ccdc.cam.ac.uk).

Acknowledgements

We thank the Australian Research Council (ARC) for financial support and Johnson-Matthey Technology Centre for the generous loan of ruthenium salts. M.G.H. holds an ARC Australian Senior Research Fellowship and M.P.C. holds an ARC Australian Research Fellowship.

References

[1] C.E. Powell, M.P. Cifuentes, J.P. Morrall, R. Stranger, M.G. Humphrey, M. Samoc, B. Luther-Davies, G.A. Heath, J. Am. Chem. Soc., in press.
[2] I.R. Whittall, A.M. McDonagh, M.G. Humphrey, M. Samoc, Adv. Organomet. Chem. 42 (1998) 291.
[3] I.R. Whittall, A.M. McDonagh, M.G. Humphrey, M. Samoc, Adv. Organomet. Chem. 43 (1999) 349.
[4] N.D. Jones, M.O. Wolf, D.M. Giaquinta, Organometallics 16 (1997) 1352.
[5] Y.B. Zhu, O. Clot, M.O. Wolf, G.P.A. Yap, J. Am. Chem. Soc. 120 (1998) 1812.
[6] C.A. McAuliffe, R.V. Parish, P.D. Randall, J. Chem. Soc. Dalton Trans. (1979) 1730.
[7] M.I. Bruce, E. Horn, J.G. Matisons, M.R. Snow, Aust. J. Chem. 37 (1984) 1163.
[8] J. Bailey, J. Inorg. Nucl. Chem. 35 (1973) 1921.
[9] K.R.J. Thomas, J.T. Lin, K.J. Lin, Organometallics 18 (1999) 5285.
[10] B. Chaudret, G. Commenges, R. Poilblanc, J. Chem. Soc. Dalton Trans. (1984) 1635.
[11] Z. Otwinowski, W. Minor, in: C.W. Carter, Jr., R.M. Sweet (Eds.), Methods in Enzymology, Academic Press, New York, 1997, p. 307.
[12] P. Coppens, in: F.R. Ahmed, S.R. Hall, C.P. Huber (Eds.), Crystallographic Computing, Munksgaard, Copenhagen, 1970, p. 255.
[13] S. Mackay, C.J. Gilmore, C. Edwards, N. Stewart, K. Shankland, MAXUS: Computer Program for the Solution and Refinement of Crystal Structures, Nonius, The Netherlands, MacScience, Japan and The University of Glasgow, UK, 1999.
[14] P.T. Beurskens, G. Admiraal, W.P. Bosman, S. Garcia-Granda, R.O. Gould, J.M.M. Smits, C. Smykalla, PATTY: the DIRDIF program system, Technical Report of the Crystallographic Laboratory, University of Nijmegen, The Netherlands, 1992.
[15] TEXSAN: Single Crystal Structure Analysis Software, Version 1.8, Molecular Structure Corporation, The Woodlands, TX, 1997.
[16] D.J. Watkin, C.K. Prout, J.R. Carruthers, P.W. Betteridge, R.I. Cooper, Crystals, Issue 11, Chemical Crystallography Laboratory, Oxford, UK.
[17] M. Sheik-Bahae, A.A. Said, T. Wei, D.J. Hagan, E.W. van-Stryland, IEEE J. Quant. Electron. 26 (1990) 760.
[18] K.R.J. Thomas, J.T. Lin, Y.S. Wen, Organometallics 19 (2000) 1008.
[19] J.G. Rodriguez, M. Gayo, I. Fonseca, J. Organomet. Chem. 534 (1997) 35.
[20] A. Hradsky, B. Bildstein, N. Schuler, H. Schottenberger, P. Jaitner, K.H. Ongania, K. Wurst, J.P. Launay, Organometallics 16 (1997) 392.
[21] S. Achar, C.E. Immoos, M.G. Hill, V.J. Catalano, Inorg. Chem. 36 (1997) 2314.
[22] J.G. Rodriguez, M. Gayo, I. Fonseca, J. Organomet. Chem. 534 (1997) 35.
[23] A. Das, H.C. Bajaj, M.M. Bhadbhade, J. Organomet. Chem. 544 (1997) 55.
[24] J.A. Mata, E. Peris, R. Llusar, S. Uriel, M.P. Cifuentes, M.G. Humphrey, M. Samoc, B. Luther-Davies, Eur. J. Inorg. Chem. (2001) 2113.
[25] I.S. Lee, Y.K. Chung, J. Mun, C.S. Yoon, Organometallics 18 (1999) 5080.
[26] D. Touchard, P. Haquette, N. Pirio, L. Toupet, P.H. Dixneuf, Organometallics 12 (1993) 3132.
[27] A.M. McDonagh, I.R. Whittall, M.G. Humphrey, B.W. Skelton, A.H. White, J. Organomet. Chem. 519 (1996) 229.
[28] R.H. Naulty, A.M. McDonagh, I.R. Whittall, M.P. Cifuentes, M.G. Humphrey, S. Houbrechts, J. Maes, A. Persoons, G.A. Heath, D.C.R. Hockless, J. Organomet. Chem. 563 (1998) 137.
[29] S.K. Hurst, M.P. Cifuentes, J.P.L. Morrall, N.T. Lucas, I.R. Whittall, M.G. Humphrey, I. Asselberghs, A. Persoons, M. Samoc, B. Luther-Davies, A.C. Willis, Organometallics 20 (2001) 4664.
[30] J.R. Carruthers, D.J. Watkin, Acta Crystallogr., Sect. C A35 (1979) 698.